AD-A143 401 THE EFFECTS OF POROUS MATERIAL ON MICROBUBBLE SKIN FRICTION REDUCTION..(U) PENNSYLVANIA STATE UNIV UNIVERSITY PARK APPLIED RESEARCH LAB.. 1/1

UNCLASSIFIED N K MADAVAN ET AL. 09 DEC 83 F/G 20/4 NL

END

FILMED

DTIC

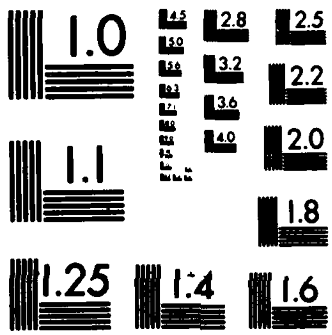

MICROCOPY RESOLUTION TEST CHART
NATIONAL BUREAU OF STANDARDS-1963-A

PHOTOGRAPH THIS SHEET

AD-A143 401

DTIC ACCESSION NUMBER

LEVEL

INVENTORY

Rpt. No. ARL/PSU/TM-83-202
Contract N00014-81-C-0481

DOCUMENT IDENTIFICATION

9 Dec '83

DISTRIBUTION STATEMENT A
Approved for public release;
Distribution Unlimited

DISTRIBUTION STATEMENT

ACCESSION FOR		
NTIS	GRA&I	☒
DTIC	TAB	☐
UNANNOUNCED		☐
JUSTIFICATION		
BY		
DISTRIBUTION /		
AVAILABILITY CODES		
DIST	AVAIL AND/OR SPECIAL	
A/1		

DISTRIBUTION STAMP

DTIC
ELECTE
JUL 26 1984
S D
D

DATE ACCESSIONED

DATE RETURNED

84 07 25 189

DATE RECEIVED IN DTIC

REGISTERED OR CERTIFIED NO.

PHOTOGRAPH THIS SHEET AND RETURN TO DTIC-DDAC

DTIC FORM 70A DEC 83 DOCUMENT PROCESSING SHEET

PREVIOUS EDITION MAY BE USED UNTIL STOCK IS EXHAUSTED.

THE EFFECTS OF POROUS MATERIAL ON MICROBUBBLE SKIN FRICTION REDUCTION

N. K. Madavan, S. Deutsch and
C. L. Merkle

Technical Memorandum
File No. TM 83-202
9 December 1983
Contract N00014-81-C-0481

Copy No. 21

The Pennsylvania State University
Intercollege Research Programs and Facilities
APPLIED RESEARCH LABORATORY
Post Office Box 30
State College, Pa. 16801

NAVY DEPARTMENT

NAVAL SEA SYSTEMS COMMAND

THE EFFECTS OF POROUS MATERIAL ON MICROBUBBLE SKIN FRICTION REDUCTION

N. K. Madavan, S. Deutsch and
C. L. Merkle

Technical Memorandum
File No. TM 83-202
9 December 1983
Contract N00014-81-C-0481

Copy No. 21

The Pennsylvania State University
Intercollege Research Programs and Facilities
APPLIED RESEARCH LABORATORY
Post Office Box 30
State College, PA 16801

NAVY DEPARTMENT

OFFICE OF NAVAL RESEARCH

UNCLASSIFIED

SECURITY CLASSIFICATION OF THIS PAGE (When Data Entered)

REPORT DOCUMENTATION PAGE		READ INSTRUCTIONS BEFORE COMPLETING FORM
1. REPORT NUMBER TM 83-202	2. GOVT ACCESSION NO.	3. RECIPIENT'S CATALOG NUMBER
4. TITLE (and Subtitle) THE EFFECTS OF POROUS MATERIAL ON MICROBUBBLE SKIN FRICTION REDUCTION		5. TYPE OF REPORT & PERIOD COVERED Technical Memorandum
		6. PERFORMING ORG. REPORT NUMBER
7. AUTHOR(s) N. K. Madavan, S. Deutsch and C. L. Merkle		8. CONTRACT OR GRANT NUMBER(s) N00014-81-C-0481
9. PERFORMING ORGANIZATION NAME AND ADDRESS Applied Research Laboratory Post Office Box 30 State College, PA 16804		10. PROGRAM ELEMENT, PROJECT, TASK AREA & WORK UNIT NUMBERS
11. CONTROLLING OFFICE NAME AND ADDRESS Office of Naval Research, Code 432 800 North Quincy Street Arlington, VA 22217		12. REPORT DATE 9 December 1983
		13. NUMBER OF PAGES 27
14. MONITORING AGENCY NAME & ADDRESS(if different from Controlling Office) Naval Sea Systems Command, Code NSEA-63R31 Department of the Navy Washington, DC 20362		15. SECURITY CLASS. (of this report) Unclassified
		15a. DECLASSIFICATION DOWNGRADING SCHEDULE

16. DISTRIBUTION STATEMENT (of this Report)

Approved for public release. Distribution unlimited.
Per NAVSEA -

17. DISTRIBUTION STATEMENT (of the abstract entered in Block 20, if different from Report)

18. SUPPLEMENTARY NOTES

19. KEY WORDS (Continue on reverse side if necessary and identify by block number)

20. ABSTRACT (Continue on reverse side if necessary and identify by block number)

Previous results have shown that the injection of a high concentration of microbubbles into a turbulent boundary layer can produce sizeable skin friction reductions. The present paper investigates the role of the porous material in this phenomenon. A variety of different porous surfaces have been tested: a series of sintered metal plates with widely different pore sizes; a specially constructed porous material, composed of plastic

DD FORM 1 JAN 73 1473 EDITION OF 1 NOV 65 IS OBSOLETE

UNCLASSIFIED

SECURITY CLASSIFICATION OF THIS PAGE (When Data Entered)

Subject: The Effects of Porous Material on Microbubble Skin Friction Reduction

References: See Page 17

Abstract: Previous results have shown that the injection of a high concentration of microbubbles into a turbulent boundary layer can produce sizeable skin friction reductions. The present paper investigates the role of the porous material in this phenomenon. A variety of different porous surfaces have been tested: a series of sintered metal plates with widely different pore sizes; a specially constructed porous material, composed of plastic strips; and two different porous section lengths. The effects of gravity were determined by changing the orientation of the porous surface with respect to the boundary layer. A notable conclusion is that the skin friction reduction is not critically related to the characteristics of the porous material. Sizeable C_f reductions are observed with all surfaces. One important difference is that the amount of air required to produce a given C_f reduction can be decreased at lower speeds by proper selection of the porous surface. Materials with larger pore size, and smaller surface area perform best at the low speeds. At the higher speeds, the smaller pore size materials produced larger C_f reductions. Gravitational effects are shown to be essentially the same for all porous materials.

Introduction

Methods for reducing the drag forces generated by the motion of hydrodynamic vehicles are important for more efficient operation and improved performance. Drag forces can be subdivided into the separate categories of form drag, pressure drag, and viscous drag. The relative importance of these several components depends upon the vehicle size, type, and design, but in general there are applications for which each is significant. The attention in the present paper is limited to viscous (skin friction) drag reduction in high Reynolds number boundary layers. This is an area which has been the subject of considerable research in recent years. Approaches such as laminar flow control through heating, cooling, suction, and body shaping, as well as turbulent flow control through the use of polymer additives, compliant coatings, and specially fabricated surface geometries which lead to a net reduction in skin friction have been considered. Recent summaries of much of the work in this area are given in the volume by Hough[1] and the review papers by Bushnell and co-workers[2,3].

In the present paper we consider an alternative, and relatively new, concept for reducing skin friction: the injection of very small gas bubbles ("microbubbles") into turbulent, liquid boundary layers. McCormick and Bhattacharyya[4] reported observing drag reductions on a towed body of revolution when current was allowed to produce hydrogen bubbles in the boundary layer through electrolysis. Soviet researchers[5-8] have also reported experiments on the effect of microbubbles on turbulent boundary layers. Instead of using electrolysis, they produced microbubbles by injecting gas into the boundary layer through a porous section of the surface. Their measurements showed that significant reductions in skin friction could be achieved in the region downstream of the injection station. Most recently the authors have also reported similar observations[9]. Whereas the results reported in Ref. 4 were for an axisymmetric body which included the combined effects of form and skin friction drag in an unknown ratio, the more recent experiments[5-9] were for a flat plate geometry in which skin friction effects were isolated. Both the experiments of the present authors and those of the Soviet researchers indicate that microbubble injection can produce skin friction reductions of as much as 80%. Reductions of this magnitude are clearly of interest for a wide range of applications.

Because the microbubble concept is relatively new, the range of parameters for which skin friction reduction can be observed has not yet been fully documented. The primary variables which have been investigated are the airflow rate and the free-stream velocity (boundary layer Reynolds number). The purpose of the present paper is to investigate the effect of changing the characteristics of the porous surface. Results are presented for variations in both the pore size and the size and type of the porous material. The intent of the study is to determine if the observed skin friction reduction is critically dependent on the characteristics of the porous surface. The results show that it is not. Substantial C_f reductions were observed for all surfaces tested. The amount of reduction did, however, vary with surface characteristics suggesting that some optimization of the air flow rate is possible. The pursuit of such an optimization would be of direct interest for practical applications.

The paper begins with a brief description of the experimental facility and technique. This is followed by a description of the types of porous materials used, their methods of construction, and surface characteristics.

The skin friction measurements behind each of these sections are then presented. Variations in the pore size, type of porous material, gravitational direction and porous section size are examined. The mechanics by which bubbles are formed in a high shear layer are then reviewed in light of the observed results, and the major conclusions are summarized in the final section.

Experimental Setup and Test Procedure

The experiments were performed in the rectangular test section of the 12-inch water tunnel at The Pennsylvania State University. The dimensions of the rectangular section are 508 mm × 114 mm × 762 mm long. The test plate was mounted in one wall of the test section and was composed of a porous section 178 mm long followed by an instrumented force balance 254 mm long. The width of both the porous section and the force balance was 102 mm. The tunnel speed was continuously variable from 0-20 m/s; the experiments reported herein ranged between 5 and 17 m/s. At these velocities, a virtual origin of the turbulent boundary layer was determined to lie some 180 mm upstream of the leading edge of the porous section[9]. A schematic of the test configuration is shown in Fig. 1.

The tunnel has several features which are of particular importance to the present experiment. For example, the section can be rotated through 90° intervals. With the plate mounted on the lower wall of the tunnel (hereafter referred to as the "plate-on-bottom" position) the effect of buoyancy tends to cause the microbubbles to rise out of the boundary layer. Of course, the extent of this rise depends upon the free-stream velocity. By rotating the test section through 180°, so that the plate is on the upper wall ("plate-on-top") the buoyancy forces tend to retain the bubbles in the boundary layer. This allows the consequent effect of gravity to be evaluated, an effect that appears particularly important in a study of pore-size sensitivity.

A second feature of the tunnel that is useful in the present context is a bypass system which removes a substantial fraction of the recirculating water from the closed circuit tunnel and replaces it with fresh water. This bypass system allowed continuous operation for extended periods (20-30 minutes was common) without collecting excess amounts of air in the free-stream.

Integrated skin friction was determined from the floating element force balance that was mounted on four legs and was instrumented with a strain gauge. To eliminate seal problems, the strain gauge was water-proofed and the space under the floating element was filled with water. The force balance was dry-calibrated by a pulley and weights arrangement. The resulting calibration exhibited excellent linearity over the force range of interest. The lower limit on tunnel velocity was determined by the minimum sensitivity of the instrumented balance. The maximum velocity was determined by the maximum allowable force on the plate.

The flow parameters of interest in the present study are the tunnel test section velocity, the injected gas flow rate, and the integrated skin friction force. The test section velocity was determined from the pressure drop across the tunnel contraction section; the injection gas flow rate was determined from a turbine flowmeter and a pressure transducer; and the integrated skin friction was determined from the calibrated strain gauge as noted earlier. All flow parameters were displayed on digital voltmeters and simultaneously recorded on digital oscilloscopes equipped with floppy disks. During each run, the airflow was gradually increased from zero to the maximum attainable value and then reduced back to zero again with care being taken to ensure that the no-air drag returned to its original value. (Maximum airflow was dictated by stress limitations on the plate confinement system when the small porosity plate was used and by the maximum volumetric capability of the air supply system for the remaining plates.) The tunnel velocity was manually held at a preselected, fixed value during the entire run. Data were acquired by reading the voltmeters at various airflow settings, or by recording and storing entire runs on the oscilloscopes for later computerized reduction. The latter procedure allowed 2048 data samples to be obtained during each run. During data reduction these samples were placed in appropriate airflow "bins" and averaged to obtain individual data points. These automated data acquisition runs were approximately seven minutes in duration.

Description and Characteristics of Porous Material

The porous material used in the original experiments[9] was a sintered stainless steel plate, 3 mm thick, manufactured by Mott Metallurgical Corporation for use as a filter. The filter chosen was capable of trapping 0.5 μm particles (nominally 5 μm pore size). In the present series ot experiments, the filter size was used as a parameter. Filter sizes tested included 0.5 μm, 5 μm, 10 μm, 50 μm and 100 μm. Because of the manufacturing process, the pore sizes in these materials are quite widely distributed, and the flow passages are winding and tortuous rather than being uniform and well-defined. Scanning electron microscope (SEM) photographs of three different filter sizes (0.5, 5 and 100 μm) are shown in Fig. 2 and give some indication of the pore size and spacing.

A second type of porous material was also used for microbubble injection. This material was modeled after the porous materials used in Refs. 5-8, and contained a well-defined, regular pattern of holes with long straight passages through which the gas traversed before entering the water boundary layer. This porous section was constructed from a large number of plastic strips 0.4 mm thick, 13 mm wide and 99 mm long. A series of parallel lines were scribed on one side of each piece by means of a laser as shown in Fig. 3. These scratches were nominally 80 μm deep × 80 μm wide, triangular in shape, and spaced on 180 μm centers. Following this, the scratched plates were stacked, scratched-side-to-smooth-side, on two pins (see Fig. 3) until enough had been assembled to form a porous section 178 mm long × 99 mm wide × 13 mm thick. The process was completed by placing the assembly under compression so that each triangular groove formed a long (13 mm) narrow passageway through the assembled block. To ensure that the assembled section was reasonably smooth on the flow side, the strips were pre-assembled on the pins, and milled smooth on one side. Following disassembly, the plates were scratched and reassembled, being careful to preserve the order and orientation of each piece. Milling prior to laser scratching prevented the closing of pores following assembly. Microscope inspection of the completed assembly showed a uniform surface porosity and a reasonable surface smoothness, although a small percentage (around 20%) of holes appeared blocked or partially so.

As a further means of characterizing the porous materials, their Δp-airflow behavior is given on Fig. 4. These data are for air injection into the tunnel and so are representative of actual conditions during the experiment. Most notable is the fact that it takes a substantially larger pressure drop to force a given volumetric airflow through the 0.5 μm material than through any of the others. In particular, the 5 μm filter and the 100 μm filter have relatively similar Δp-flow characteristics, while the characteristics of the 0.5 and 5 μm filters are quite different. In an actual application, the Δp required to obtain a given volumetric flow rate of gas could be minimized by using one of the larger pore size materials if such a choice did not prove deleterious to the drag reduction characteristics.

Reynolds Number - C_f Variation in the Absence of Bubbles

The variation of the integrated skin friction coefficient in the absence of microbubbles is shown on Fig. 5 as a function of Reynolds number. These Reynolds numbers are based on the distance from a virtual origin to the trailing edge of the force balance. The location of the virtual origin was determined[9] from laser Doppler measurements of the undisturbed boundary layer profiles. For comparison, a skin friction correlation based on a "best fit" to classical boundary layer data[10] is also shown on Fig. 5. This comparison requires that two lengths, l_1 and l_2, be defined. These lengths correspond to the distances between the virtual origin and the leading edge and trailing edge of the force balance, respectively.

The no-air skin friction data on Fig. 5 are presented as a mean line drawn through some 200 data points taken throughout a two-year period. During this time the apparatus was disassembled and re-assembled multiple times, measurements were taken downstream of various types of porous plates, and both gravitational orientations were used. The tolerance bands given in the shows that the C_f reduction again occurs more rapidly at low airflow rates with the larger pore size materials.

Effects of Length of Porous Plate

Figures 10 and 11 also contain comparisons of the effect of changes in the length of the injection section. These figures include data for the 50 μm filter with the standard length of 180 mm as well as with a shorter length of 45 mm. (Note all sets of data are normalized by the area of the 180 mm plate.) The data on Fig. 10 indicate that at 10.7 m/s the two injection lengths give almost the same skin friction reduction with perhaps a slight advantage for the shorter section. At 4.6 m/s the shorter injection length gives noticeably more C_f reduction at the lower airflow rates as is seen on Fig. 11. By combining these results with those reported in Ref. 9 where injection lengths of 180 mm and 90 mm were compared for the 0.5 μm filter, it can be stated more generally that shortening the injection section has no adverse effect on the skin friction reductions. Optimization of the length of the porous section may afford more efficient use of the bubbles (the same C_f reductions with smaller airflow rates) at the lower tunnel speeds.

Comparison of Stacked Plates and Sintered Metal

Results of testing the stacked plates described on Fig. 4 are shown in Figs. 12 and 13. Only limited data are available with this porous material. These are compared with the 100 μm filter data for the plate-on-bottom configuration. Figure 12 shows the comparison at 14.4 m/s while figure are drawn so as to include all data points (except one). These bands lie within ± 5% of the classical data at higher Reynolds numbers, and ± 8% at the lower Reynolds numbers. The somewhat larger tolerance at the lower Reynolds numbers arises because the force on the balance is becoming smaller at these lower speeds.

Pore Size Variations--Plate on Top

The results with microbubbles are presented in terms of a normalized skin friction, C_f/C_{f_o}, versus a nondimensional airflow parameter, Q/SU_∞. Here C_{f_o} is the skin friction in the absence of microbubbles, while S is the surface area of the porous material. This nondimensionalization of the airflow rate in essence relates the volumetric flow of air to that of water. (The use of the displacement thickness times the width of the porous section would be a more precise ratio of the volumetric flows, but since δ^* does not vary widely for the conditions reported here, the present constant area produces essentially the same effect.) Earlier results[9] have shown that the surface area collapses the plate-on-top data quite well for a wide range of tunnel speeds, but that it is not nearly as effective for the plate-on-bottom data. The primary reason for this is the skin friction is affected by the location of the bubbles as well as their concentration.

Figures 6 through 8 present integrated skin friction results for the plate-on-top configuration. Each figure presents data for one nominal tunnel speed and compares the effect of several filter sizes. A cursory inspection of these three figures shows that all filter sizes yield sizeable skin friction reductions at all speeds. The various filter sizes have only a minor impact on the skin friction reduction and this impact does not vary regularly with pore size. At the highest tunnel speed, 16.7 m/s, the data for the 0.5 μm plate show somewhat larger reductions in C_f than do the data from the 100 μm plate (see Fig. 6). Figure 7 shows a similar trend at 11.2 m/s. By contrast, Fig. 8 shows the 0.5 μm filter is inferior to the others at 4.8 m/s, except possibly at the highest airflow rates. This figure also suggests that a given amount of drag reduction can be obtained at smaller airflow rates when the larger filter sizes are used. The scatter in the data at this low speed make these observations somewhat tenuous but additional data, presented later, also support this observation.

We also note in connection with these figures that the reason the range of Q/SU_∞ varies so widely among the three velocity conditions is because of the effect of U_∞ in the denominator of the airflow parameter. The same maximum airflow rate was reached for all three speeds, but the nondimensional parameter varies over narrow limits at high speeds and wide limits at low speeds. Thus, the volumetric concentration of air in the boundary layer was smaller at the higher speeds.

Pore Size Variations--Plate on Bottom

A comparison of pore size effects with the plate on the bottom of the tunnel is given on Figs. 9 through 11. These results again show that pore size variations have a minor impact on the C_f reduction and that all pore sizes result in sizeable skin friction reductions. Figures 9 and 10 show almost no effect of pore size at 16.7 and 10.7 m/s while Fig. 11 suggests that the larger pore sizes are again preferred at 4.6 m/s. Figure 11 also

Fig. 13 is for 11.0 m/s. In both cases, the stacked plates give somewhat larger C_f reductions than does the 100 μm sintered material. Comparison with Figs. 9 and 10 suggests that the stacked plate results fall within the overall band of data obtained with the sintered metal. Although these results strengthen the previous observations that the effects of the microbubbles are only weakly dependent on the porous material, additional experiments with this porous surface appear warranted.

One important aspect of this stacked-plate data is that the regular array of well-defined flow passages lends itself to analytical modeling of the bubble formation process. Because of the regular array, the number of pores can be estimated, and, given the pressure drop across the porous material, the characteristics of the gas stream issuing from each pore can be calculated. Such estimates cannot be made for the sintered metal with its random pore size and spacing, and its tortuous flow passages. Models of the bubble formation and dynamics would appear to be imperative in extending our understanding of the microbubble boundary layer. Simple models have already been reported[11], but more detailed studies are needed.

Effects of Gravity

The results shown earlier have been replotted on Figs. 14 and 15 to show the difference between the plate-on-top and the plate-on-bottom orientations. Figure 14 shows data at 16.7 m/s for the 0.5 and 100 μm sintered plates. The darkened symbols are for the plate on the bottom, while the open symbols are for the plate on top. Both pore sizes show that the plate-on-top configuration gives slightly better results, but there is little difference between the two gravitational orientations at this speed. The results at

11.0 m/s (Fig. 15) show a substantially larger variation with plate orientation but again show no significant difference between the two filter sizes. The effects of gravity on the bubbles generated by the 100 μm porous section are about the same as on the bubbles generated with the 0.5 μm plate. These results augment previous conclusions[9] that gravity-induced bubble migration produces measurable effects over the length of the force balance at low and intermediate speeds but that this effect has nearly died out at high speeds.

Normalization of Airflow Data

As a final check on the effect of pore size, the data for all speeds and a single pore size is presented on separate figures. The results for the 0.5 μm filter are shown on Fig. 16 while those for the 100 μm filter are on Fig. 17. Figure 16 illustrates the degree to which the Q/SU_∞ normalization can collapse data for velocities ranging between 4.8 and 16.7 m/s. A similar comparison for the 100 μm plate is given on Fig. 17. Here, this normalization is found to be much less effective. (Note that the data in Figs. 16 and 17 are all for the plate-on-top configuration.) The data, when plotted in this format, show a more distinctive trend between C_f reduction and pore size than on the previous curves (similar observations can be made for the plate-on-bottom data when plotted in this fashion). Careful comparison of Figs. 16 and 17 confirms that at the higher speeds the 0.5 μm filter performs better, while at lower speeds the 100 μm filter performs best.

Summary and Conclusions

The primary conclusion of the present study is that the skin friction is strongly influenced by the presence of microbubbles, irregardless of the characteristics of the porous material through which the bubbles are generated. This secondary nature of changes in pore size on the drag characteristics of the microbubble boundary layer is somewhat surprising. Intuitively, one might expect that pore size changes would lead to bubble size changes, and that the altered bubble sizes would be incapable of reducing skin friction. The data do not support this. Since the data show that the porous material has little effect on skin friction, it would appear that it also must have little effect on the bubble size. That is to say, the bubble size appears to be controlled largely by the characteristic scales in the turbulent boundary layer. Although data for bubble formation in a flowing liquid is quite sparse, the only two available studies[12,13] (which are for experimental conditions quite different than those in the present experiment), also support this viewpoint. References 12 and 13 show that bubble formation from single pores of large size (800 μm to 10 mm) produces bubble diameters, D, that are independent of pore size, d, at high flow rates,

$$D \sim \sqrt{Q/U_\infty}$$

and that are only weakly dependent on pore size at low flow rates,

$$D \sim d^{1/3} \quad .$$

These single pore results would appear to explain the relative insensitivity to pore size in the present results.

Even though the porous material does not have a dramatic effect on the skin friction characteristics, the effects which it does have are quite interesting. Particularly noteable is the manner in which the skin friction shifts with velocity for the various materials. These differences are most clearly seen when the composite results for all velocities for a given porous surface are plotted together. For example, the results for the 0.5 μm plate (Fig. 16) collapse into a single line when plotted against Q/SU_∞, but the results for the 100 μm plate (Fig. 17) are widely dispersed on the same coordinates. Checks of the intermediate pore sizes (not shown) indicate that the Q/SU_∞ nondimensionalization becomes increasingly less successful as the pore size is increased. Similar response to changes in the length of the porous section are also to be expected. These effects, not as yet understood, may become quite significant when practical aspects of the microbubble phenonenon--optimization and scale-up--are considered. The phenomena which determine the optimum pore size and which govern scale-up are clearly complex and complete documentation will require additional measurements. The effectiveness of microbubble injection depends upon the bubble sizes that are formed and their dynamics following formation. The bubble sizes are controlled by the boundary layer characteristics including its thickness, local Reynolds number, and profile shape in addition to the pore dimensions. The bubble dynamics are likewise dependent on the boundary layer characteristics as well as the bubble diameters and include variations in trajectory and in the rate at which bubbles coalesce and break up.

Acknowledgment

This work was sponsored by the Office of Naval Research under Contract Number N00014-81-K-0481.

References

(1) Hough, G. R., Viscous Flow Drag Reduction, Progress in Astronautics and Aeronautics 72, 1980.

(2) Hefner, J. H., D. M. Bushnell, R. T. Whitcomb, A. M. Cary, Jr. and R. L. Ash, "Concepts for Aircraft Drag Reduction," AGARD/VKI Special Courses on Concepts for Drag Reduction, Rhode-St-Genese, Belgium, March 1977, AGARD-R-654.

(3) Bushnell, D. M., "Turbulent Drag Reduction for External Flows," AIAA-83-0227, presented at the AIAA 21st Aerospace Sciences Meeting, Reno, VN, 10-13 January 1983.

(4) McCormick, M. E. and R. Bhattacharyya, "Drag Reduction of a Submersible Hull by Electrolysis," Naval Engineers Journal 85, 1973, pp. 11-16.

(5) Migirenko, G. S. and A. R. Evseev, "Turbulent Boundary Layer with Gas Saturation," Problems of Thermophysics and Physical Hydrodynamics (in Russian), (Novoskbirsk), Nauka, 1974.

(6) Dubnischev, Yu. N., A. R. Evseev, V. S. Sobolev and E. N. Utkin, "Study of Gas-Saturated Turbulet Streams using a Laser-Doppler Velocimeter," J. Appl. Mech. Tech. Phys. 16, No. 1, 1975, p. 114. Translated from Zhur. Prikl. Mech. Tekh. Fiz., No. 1, 1975, p. 147.

(7) Bogdevich, V. G. and A. G. Malyuga, "The Distribution of Skin Friction in a Turbulent Boundary Layer in Water beyond the Location of Gas Injection," in Investigations of Boundary Layer Control (in Russian), edited by S. S. Kutateladze and G. S. Migirenko (Thermophysics Institute Publishing House, 1976), p. 62.

(8) Bodgevich, V. G. and A. R. Evseev, "Effect of Gas Saturation on Wall Turbulence," in Investigations of Boundary Layer Control (in Russian), edited by S. S. Kutateladze and G. S. Migirenko (Thermophysics Institute Publishing House, 1976), p. 49.

(9) Madavan, N. K., S. Deutsch and C. L. Merkle, "Reduction of Turbulent Skin Friction by Microbubbles," Physics of Fluids, 1984. To appear.

(10) White, F. M., Viscous Fluid Flow, McGraw-Hill, Inc., New York, NY, 1974, pp. 468-505.

(11) Madavan, N. K., C. L. Merkle and S. Deutsch, "Numerical Investigations into the Mechanisms of Microbubble Drag Reduction," to be presented at the 1984 ASME Fluids Engineering Conference, New Orleans, February 1984.

(12) Silberman, E., "Production of Bubbles by the Disintegration of Gas Jets in Liquid," Proceedings of the 5th Midwestern Conference on Fluid Mechanics, University of Michigan, 1957, p. 263-284.

(13) Hughes, N. J., M. M. Reischman and J. M. Holzmann, "Digital Image Analysis of Two Phase Flow Data," Proceedings of the 6th Biennial Symposium on Turbulence, University of Missouri, 1979, p. 274.

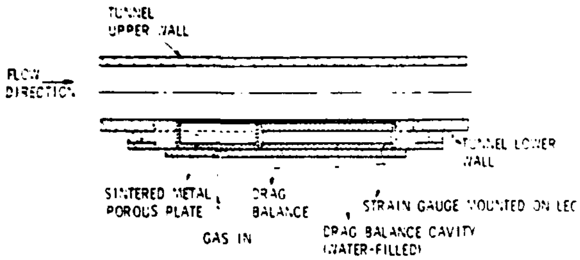

Fig. 1 Schematic of experimental setup.

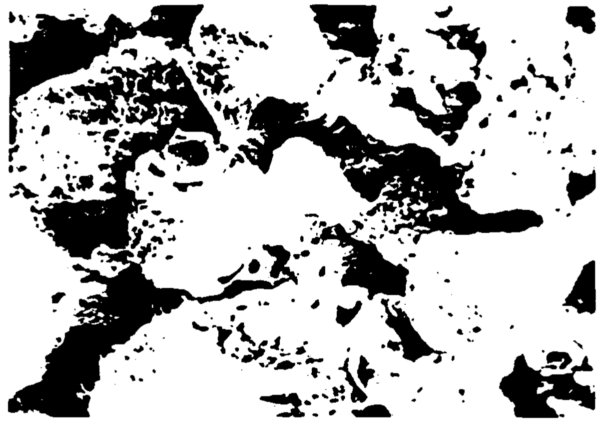

(c)

(a)

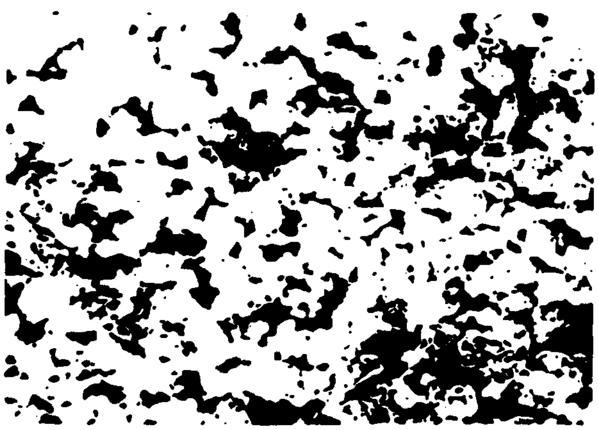

(b)

Fig. 2 Scanning Electron Microscope photographs of three different filter sizes:
(a) 0.5 μm filter, mag: 270X
(b) 50 μm filter, mag: 45X
(c) 100 μm filter, mag: 45X
Note different magnification on each figure.

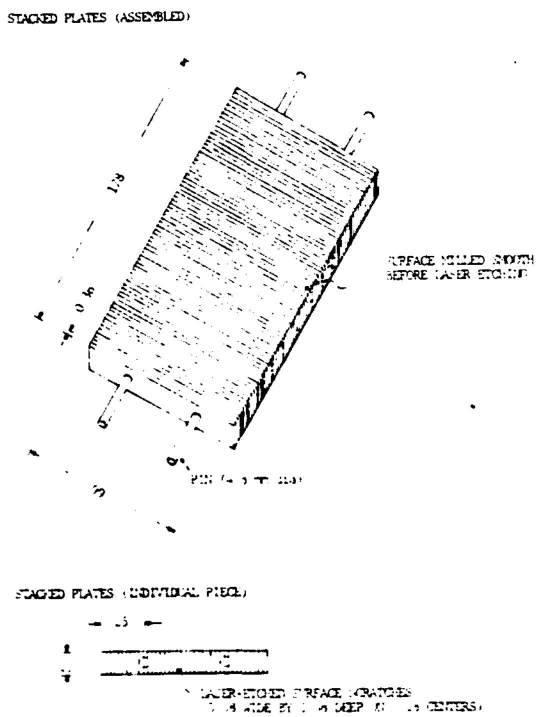

Fig. 3 Schematic of porous material fabricated from stacked plates.

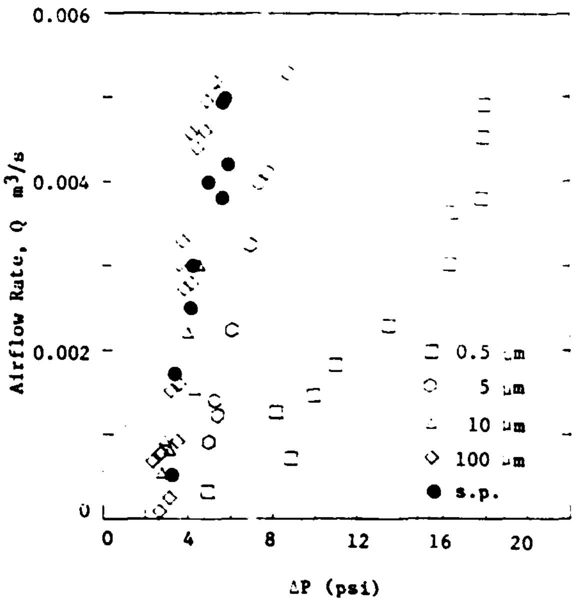

Fig. 4 Characterization of the pressure drop versus airflow rate behavior of the different porous materials.

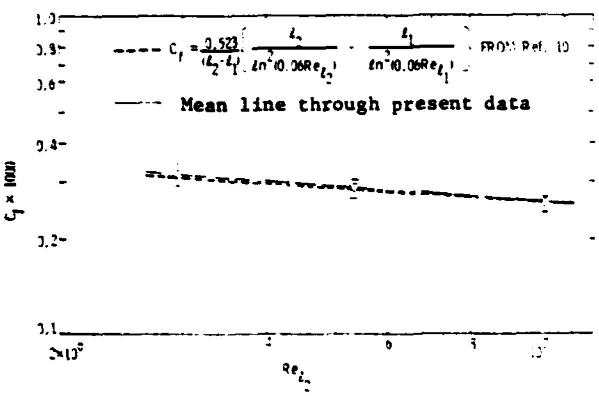

Fig. 5 Comparison of integrated skin friction measurements with classical data.

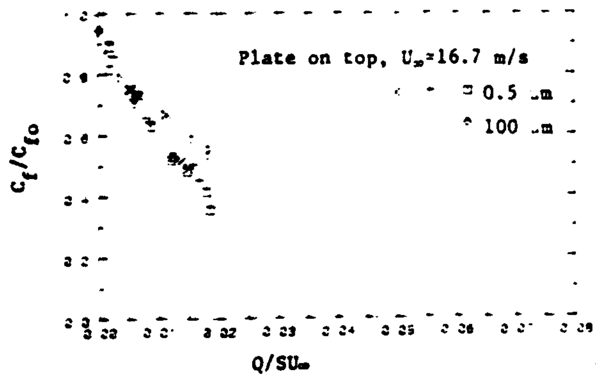

Fig. 6 Effect of pore size variation on skin friction reduction with microbubbles for plate-on-top configuration. U_∞ = 16.7 m/s

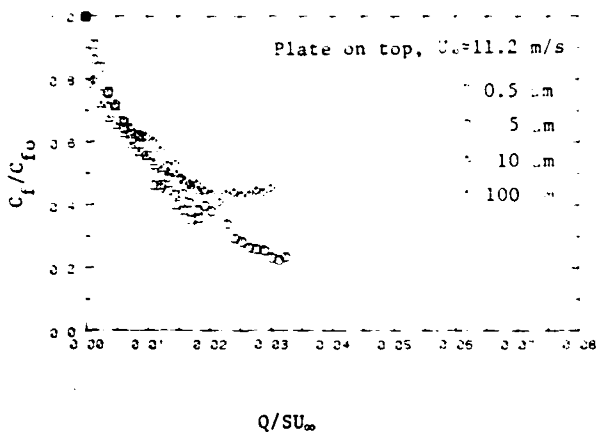

Fig. 7 Effect of pore size variation on skin friction reduction with microbubbles for plate-on-top configuration. U_∞ = 11.2 m/s

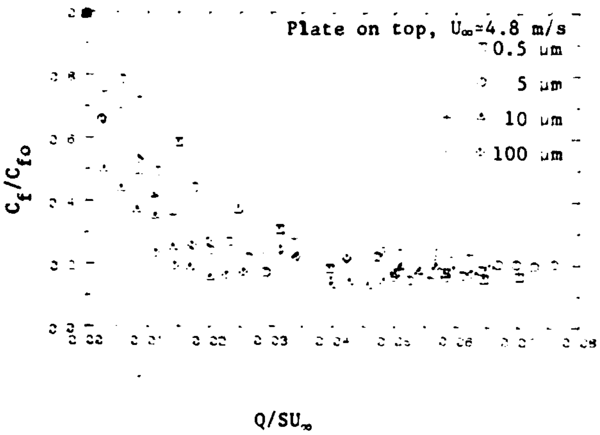

Fig. 8 Effect of pore size variation on skin friction reduction with microbubbles for plate-on-top configuration. U_∞ = 4.8 m/s

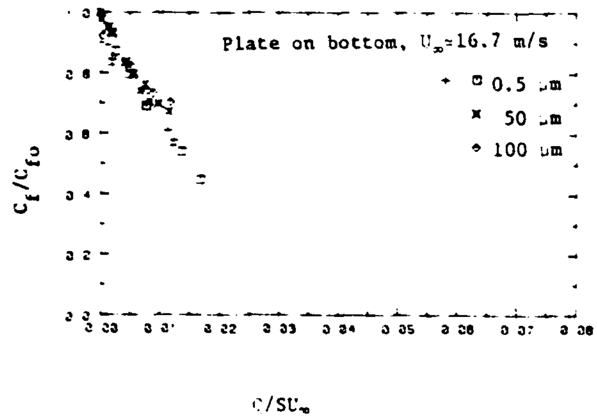

Fig. 9 Effect of pore size variation on skin friction reduction for plate-on-bottom configuration. U_∞ = 16.7 m/s

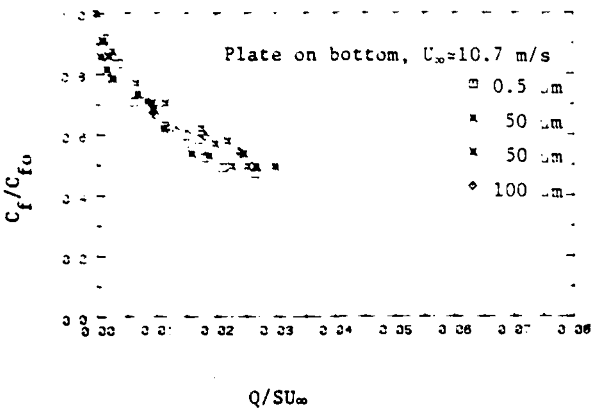

Fig. 10 Effect of pore size variation on skin friction reduction for plate-on-bottom configuration. $U_\infty = 10.7$ m/s

Darkened symbol denotes data taken with reduced length (45 mm) of injection section.

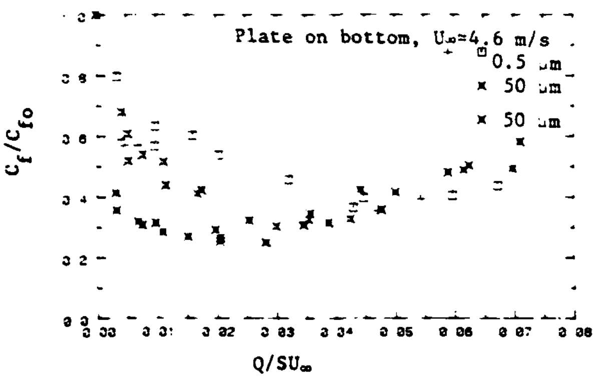

Fig. 11 Effect of pore size variation on skin friction reduction for plate-on-bottom configuration. $U_\infty = 4.6$ m/s

Darkened symbol denotes data taken with reduced length (45 mm) of injection section.

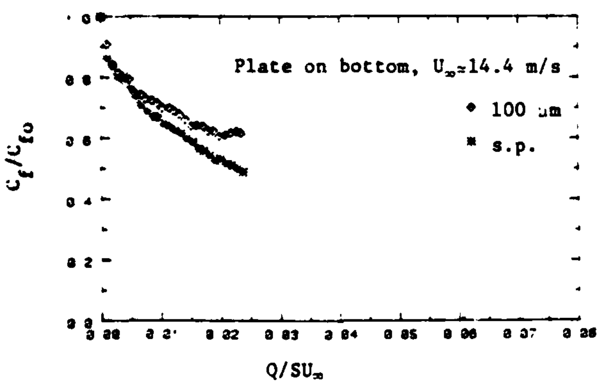

Fig. 12 Comparison of skin friction reduction with microbubbles for stacked plates and sintered materials. $U_\infty = 14.4$ m/s (s.p. denotes stacked plates)

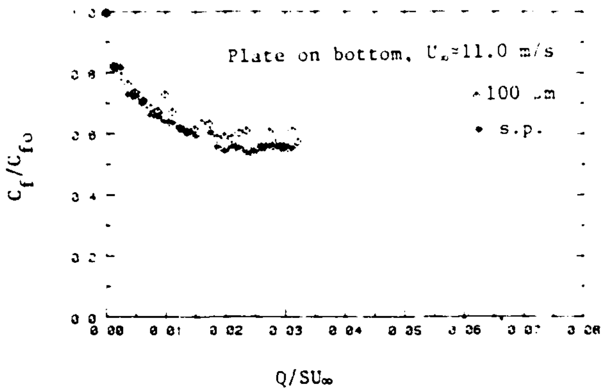

Fig. 13 Comparison of skin friction reduction with microbubbles for stacked plates and sintered materials. $U_\infty = 11.0$ m/s (s.p. denotes stacked plates)

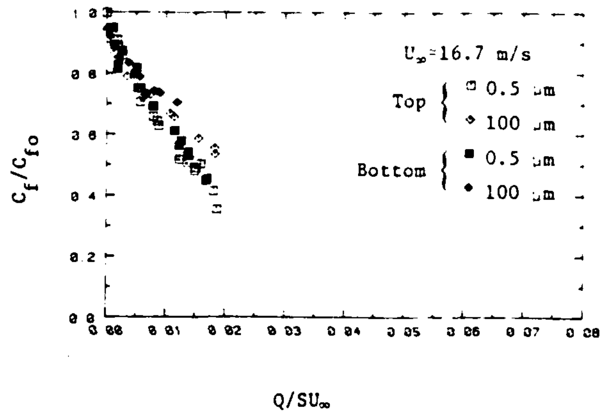

Fig. 14 Effect of gravitational direction on skin friction reduction with micro-bubbles. $U_\infty = 16.7$ m/s

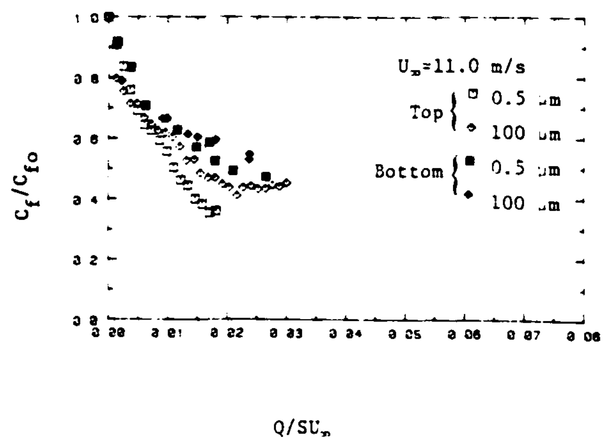

Fig. 15 Effect of gravitational direction on skin friction reduction with micro-bubbles. $U_\infty = 11.0$ m/s

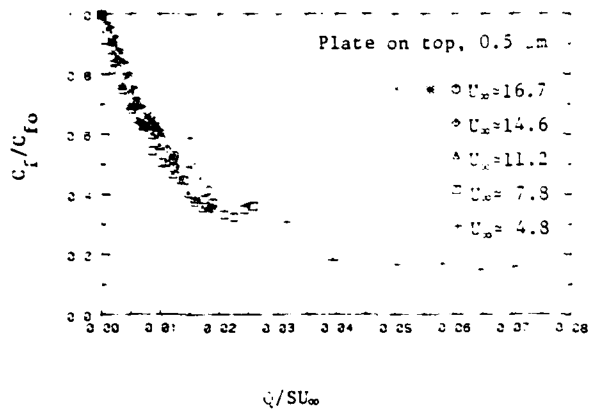

Fig. 16 Replot of skin friction data taken with microbubbles at various freestream velocities for plate-on-top configuration. 0.5 μm filter size.

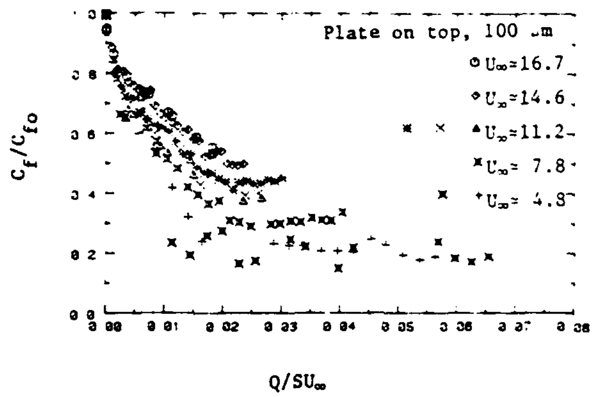

Fig. 17 Replot of skin friction data taken with microbubbles at various freestream velocities for plate-on-top configuration. 100 μm filter size.

DISTRIBUTION LIST FOR ARL UNCLASSIFIED TM No. 83-202 by N. K. Madavan, S. Deutsch and C. L. Merkle, dated 9 December 1983

Commander
Naval Sea Systems Command
Department of the Navy
Washington, DC 20362
Attn: Library
Code NSEA-09G32
(Copies 1 and 2)

Commander
Naval Sea Systems Command
Department of the Navy
Washington, DC 20362
Attn: F. Romano
Code NSEA-63R
(Copy No. 3)

Commander
Naval Sea Systems Command
Department of the Navy
Washington, DC 20362
Attn: T. E. Peirce
Code NSEA-63R31
(Copy No. 4)

Commander
Naval Sea Systems Command
Department of the Navy
Washington, DC 20362
Attn: S. M. Blazek
Code NSEA-55N
(Copy No. 5)

Commander
Naval Sea Systems Command
Department of the Navy
Washington, DC 20362
Attn: A. R. Paladino
Code NSEA-55N
(Copy No. 6)

Commander
Naval Sea Systems Command
Department of the Navy
Washington, DC 20362
Attn: W. D. Marlin
Code NSEA-931E
(Copy No. 7)

Commander
Naval Sea Systems Command
Department of the Navy
Washington, DC 20362
Attn: E. G. Liszka
Code PMS-406B
(Copy No. 8)

Commanding Officer
Naval Underwater Systems Center
Department of the Navy
Newport, RI 02840
Attn: Library
Code 54
(Copy No. 9)

Commanding Officer
Naval Underwater Systems Center
Department of the Navy
Newport, RI 02840
Attn: T. A. Davis
Code 36314
(Copy No. 10)

Commanding Officer
Naval Underwater Systems Center
Department of the Navy
Newport, RI 02840
Attn: D. Goodrich
Code 3634
(Copy No. 11)

Commanding Officer
Naval Underwater Systems Center
Department of the Navy
Newport, RI 02840
Attn: R. H. Nadolink
Code 3634
(Copy No. 12)

Commanding Officer
Naval Underwater Systems Center
Department of the Navy
Newport, RI 02840
Attn: C. N. Pryor
Code 01
(Copy No. 13)

Commanding Officer
Naval Underwater Systems Center
Department of the Navy
Newport, RI 02840
Attn: C. Hervey
Code 3634
(Copy No. 14)

Officer-in-Charge
David W. Taylor Naval Ship Research
and Development Center
Department of the Navy
Bethesda, MD 20084
Attn: M. M. Sevik
Code 19
(Copy No. 15)

Officer-in-Charge
David W. Taylor Naval Ship Research
and Development Center
Department of the Navy
Bethesda, MD 20084
Attn: J. H. McCarthy
Code 154
(Copy No. 16)

Officer-in-Charge
David W. Taylor Naval Ship Research
and Development Center
Department of the Navy
Bethesda, MD 20084
Attn: T. T. Huang
Code 1552
(Copy No. 17)

Officer-in-Charge
David W. Taylor Naval Ship Research
and Development Center
Department of the Navy
Bethesda, MD 20084
Attn: J. Shen
Code 194
(Copy No. 18)

Commander
Naval Surface Weapons Center
Department of the Navy
Silver Spring, MD 20910
Attn: G. C. Guanaurd
(Copy No. 19)

Office of Naval Research
800 North Quincy Street
Department of the Navy
Arlington, VA 22217
Attn: R. Whitehead
Code 432
(Copy No. 20)

Office of Naval Research
800 North Quincy Street
Department of the Navy
Arlington, VA 22217
Attn: M. M. Reischman
Code 432F
(Copy No. 21)

National Bureau of Standards
771.FM105
Washington, DC 20234
Attn: P. S. Klebanoff
(Copy No. 22)

National Bureau of Standards
771.FM105
Washington, DC 20234
Attn: J. M. McMichael
(Copy No. 23)

Naval Research Laboratory
Department of the Navy
Washington, DC 20390
Attn: R. J. Hansen
(Copy No. 24)

Rand Corporation
1700 Main Street
Santa Monica, CA 90406
Attn: R. King
(Copy No. 25)

Rand Corporation
1700 Main Street
Santa Monica, CA 90406
Attn: J. Aroesty
(Copy No. 26)

Rand Corporation
1700 Main Street
Santa Monica, CA 90406
Attn: C. Gazley
(Copy No. 27)

Rand Corporation
1700 Main Street
Santa Monica, CA 90406
Attn: A. R. Wazzan
(Copy No. 28)

Dynamics Technology, Inc.
22939 Hawthorne Blvd.
Suite 200
Torrance, CA 90505
Attn: W. W. Haigh
(Copy No. 29)

Dynamics Technology, Inc.
22939 Hawthorne Blvd.
Suite 200
Torrance, CA 90505
Attn: G. L. Donohue
(Copy No. 30)

Prof. W. M. Phillips
Chairman
Department of Mechanical Engineering
Purdue University
Lafayette, IN 47907
(Copy No. 31)

Dr. Robert F. Mons
Westinghouse Electric Corporation
Post Office Box 1458
Annapolis, MD 21404
(Copy No. 32)

Prof. J. L. Lumley
Sibley School of Engineering
Cornell University
Ithaca, NY 14850
(Copy No. 33)

Prof. C. L. Merkle
Dept. of Mechanical Engineering
The Pennsylvania State University
University Park, PA 16802
(Copy No. 34)

Mr. N. K. Madavan
Dept. of Mechanical Engineering
The Pennsylvania State University
University Park, PA 16802
(Copy No. 35)

Applied Research Laboratory
The Pennsylvania State University
Post Office Box 30
State College, PA 16801
Attn: B. R. Parkin
(Copy No. 36)

Applied Research Laboratory
The Pennsylvania State University
Post Office Box 30
State College, PA 16801
Attn: R. E. Henderson
(Copy No. 37)

Applied Research Laboratory
The Pennsylvania State University
Post Office Box 30
State College, PA 16801
Attn: S. Deutsch
(Copies 38, 39 and 40)

Applied Research Laboratory
The Pennsylvania State University
Post Office Box 30
State College, PA 16801
Attn: G. B. Gurney
(Copy No. 41)

Applied Research Laboratory
The Pennsylvania State University
Post Office Box 30
State College, PA 16801
Attn: Water Tunnel Files
(Copy No. 42)